MSDE

PAPER

View Article Online
View Journal | View Issue

Check for updates

Cite this: *Mol. Syst. Des. Eng.*, 2023, **8**, 756

Post engineering of a chemically stable MOF for selective and sensitive sensing of nitric oxide†

Writakshi Mandal,[a] Dipanjan Majumder,[a] Sahel Fajal,[a] Sumanta Let,[a] Mandar M. Shirolkar[b] and Sujit K. Ghosh *[ac]

Received 26th December 2022,
Accepted 1st February 2023

DOI: 10.1039/d2me00278g

rsc.li/molecular-engineering

Published on 02 februari 2023. Downloaded on 20/09/2024 12:59:19.

A hydrolytically stable luminous metal–organic framework (MOF) sensor was strategically designed for precise dual phase recognition of biologically relevant yet toxic nitric oxide (NO). Judicious utilization of the enabling post-synthetic modification (PSM) technology in chemically robust MOF-808 yielded amine decorated and highly luminescent PABA@MOF-808. The thus-prepared functionalized sensory probe was employed for sensitive detection of NO in both aqueous and gaseous phases in a selective manner. An exclusive fluorogenic "turn-off" response was observed for NO over other relevant reactive nitrogen and oxygen species (RNS and ROS) with high quenching efficiency *via* deamination reaction as the *modus operandi*. The potency of PABA@MOF-808 toward accurate detection of NO was further punctuated by a high K_{sv} value (6.10×10^3 M^{-1}) and an exceptional limit of detection (LOD) value of 0.715 μM (21.45 ppb). Additionally, the underlying sensing mechanism was disseminated with the help of experimental data as well as theoretical insights. Pertaining to processability toward practical implementation, a flexible self-standing mixed-matrix membrane (MMM) of PABA@MOF-808 was further devised for efficient sensing of NO in both water medium and vapor phase.

Design, System, Application

Nitric oxide (NO), in spite of being a biologically relevant molecule, prevails as a noxious environmental pollutant and can cause ecological disruption. A surplus of NO levels in the atmosphere can induce respiratory sickness to mankind as well as acceleration of ozone depletion. Therefore, it becomes topical to develop high efficiency NO sensors featuring high sensitivity, low detection limits and easy processability pertaining to practical application. However, the literature reports addressing this particular issue are few and far in between. In this work, we show that strategic utilization of post-synthesis structural engineering can lead to the fabrication of a luminous metal–organic framework (MOF) based superior NO sensor. We demonstrate that tethering of specific functional groups on the pore surface ensures selective interaction of guest molecules while the fluorogenic read-out signal is perturbed by chemical reaction with the targeted analyte.

Introduction

Nitric oxide is produced naturally by oxidation of amino acids (L-arginine to L-citrulline) with a heme-containing enzyme known as nitric oxide synthase (NOS).[1] Nitric oxide (NO) works as a retrograde neurotransmitter, allows the blood flow in the brain and also has significant roles in intercellular signaling.[1,2] It can act as a regulatory agent in various physiological and pathological processes, *e.g.*, leukocyte adhesion inhibition, bronchodilation, renal functioning, *etc.*[1,3] Owing to the immense importance of NO in various biological signalling processes, it has attracted much attention of biologists, chemists, and medical researchers.[4] On the other hand, excess concentration of NO in aqueous medium and air causes deleterious consequences to the living systems, especially for human beings.[5,6] Therefore, considering both the importance and adverse impacts of nitric oxide, selective and sensitive monitoring of NO from a water medium as well as a vapour phase has become an imperative research topic, which is highly relevant to practical environmental surveillance. Moreover, from the perspective of various biological and pathological processes the selective identification of NO is also vital. However, owing to its very brief lifetime along with high diffusivity and

[a] *Department of Chemistry, Indian Institute of Science Education and Research (IISER) Pune, Dr. Homi Bhabha Road, Pashan, Pune 411008, India. E-mail: sghosh@iiserpune.ac.in; Web: https://skg-lab.acads.iiserpune.ac.in/home*
[b] *Symbiosis Centre for Nanoscience and Nanotechnology (SCNN), Symbiosis International (Deemed University) (SIU), Lavale, Pune 412115, India*
[c] *Centre for Water Research (CWR), Indian Institute of Science Education and Research (IISER) Pune, Dr. Homi Bhabha Road, Pashan, Pune 411008, India*
† Electronic supplementary information (ESI) available. See DOI: https://doi.org/10.1039/d2me00278g

This journal is © The Royal Society of Chemistry and IChemE 2023

Published on 02 februari 2023. Downloaded on 20/09/2024 12:59:19.

volatility it is extremely difficult to precisely recognize NO.[1,7] In this view, to date, several efforts have been made to develop effective sensory materials for the specific recognition of nitric oxide from different media. Also, various methods like calorimetry, electron paramagnetic resonance, electrochemical and chemiluminescence have been applied for the detection of NO.[1,7] However, all these methods exhibited several limitations such as time consuming, low efficiency, expensive, complex techniques, *etc.*[7] In regard with this, recently, fluorescence based detection methods have been considered as promising over others due to their unique properties including quick response time, easy and simple economical operation, large Stokes shifts, high sensitivity towards real-time monitoring and non-invasive nature.[8,9] Moreover, the optimal fluorescence probe should show a notable variation in fluorescence intensity along with high selectivity even in the presence of interfering analytes.[10] Owing to these advantages, numerous small organic molecule and metal based fluorescent probes have been developed and further utilized for the detection of various environmentally relevant toxic species. Importantly, to our particular interest, *ortho*-diamine based fluorescent probes and metal based complexes are widely used for NO sensing.[11–16] However, in spite of substantial progress in the development of *in vivo* targeted synthetic probes, there are several intrinsic limitations including the water solubility and hydrolytic instability of organic molecule based probes, which restrict their large-scale real-time sensing application. In order to overcome these shortcomings, development of suitable materials for efficient detection of toxic species such as NO is the primary focus of current research in this domain.

In this context, metal–organic frameworks (MOFs) or porous coordination polymers (PCPs) have emerged as a propitious and unique class of materials with crystalline architectures.[17] MOFs are porous solid materials, made up by coordination assembly of organic ligands and metal nodes or clusters, where organic ligands and metal clusters can be functionalized in line with the desired applications.[18–20,57] Moreover, because of their unique characteristics such as highly porous nature, large surface area, tunable functionality, and structure–property correlation, MOFs have appeared as candidate target specific guest approachable host systems, and therefore received intense attention in different leading applications including gas storage, chemical separation, catalysis, electrochemistry, biology and most importantly sensing.[20–22] That being said, luminescent MOFs (LMOFs), a subclass of MOFs, have extensively been studied for the chemical sensing application. Incorporating intensely emissive guests, d^0 or d^{10} metal cations, and prudent selection of π-electron rich organic linkers are just a few of the deliberate strategies that have made LMOFs the frontrunner in the identification of numerous toxic substances.[23–25] Lower detection limits and quick response mechanisms are made possible by the combined advantages of molecular sieving and confinement effect in porous MOFs. These advantages include significant improvements in selectivity as well as host–guest interactions that initiate signal transduction in the counter-reaction to a specific analyte.[26,27] Furthermore, the heterogeneous nature of MOFs makes them simple to recover for recycling purposes in such an application.[28] In addition, the facile design strategy with the judicious choice of linkers to incorporate specific functionality into the framework provided high selectivity and sensitivity to the host framework towards the incoming analyte.[29] In this line, linker modulation imparts a great impact in the design of luminescent MOFs which can be easily achieved *via* post-synthetic modification of the organic ligand or especially the metal cluster of MOFs.[30,31,56]

The capability to detect low concentrations of nitric oxide is of emerging importance. In order to monitor the water quality and air quality index, it is best to identify harmful NO in water and vapor as early as possible, before the concentrations increase, collect in the local environment, and result in significant harm.[14,32–35] In the literature, the majority of the NO sensing studies depend upon electrochemical measurement, which requires exclusive expert personnel, complex operation and high cost.[36–39] This has largely limited the versatile easy sensing application. Therefore, techniques that can offer simple and economical ways to detect NO with high sensitivity and selectivity and more importantly based on potable instrumentation is highly desirable. On the other hand, a material for target specific analyte detection in aqueous media must first be stable in water in order to be used in practice.[9] Along with this, considering the fact that the chemical environment of NO containing vapour is acidic, it is particularly important for the probe to be highly stable under extreme acidic conditions. Furthermore, in the above mentioned reports, the NO sensing studies have been done with the typical powder form, which further restricts the real-time practical monitoring. Therefore, development of a highly efficient, chemically and hydrolytically stable luminescent MOF-based sensor in the form of a device (such as a membrane) for the selective and sensitive detection of nitric oxide species is highly desirable.

With this aim along with considering all the aforementioned discussion, in this work we have chosen Zr(IV)-based MOF-808 as a promising platform for developing an efficient sensor for NO detection by rational post integration of specific functionality, owing to its following unique properties. MOF-808 is a well-known highly chemically, thermally and hydrolytically stable Zr(IV) metal cluster based porous MOF.[40,41] The presence of a benzene core ligand together with d^{10} metal cations makes MOF-808 a luminescent probe, which is further utilized as a sensory material.[42,43] Moreover, the Zr_6-oxo cluster of MOF-808 offers tunable functionality in the framework by allowing simple yet versatile, facile induction of diverse functional moieties in its secondary building unit (SBU) by exchanging the formate linker.[42–45] Furthermore, MOF-808 was found as an ideal MOF candidate for the fabrication of mixed-matrix-membranes (MMMs), because of its special cluster coordination and the ensuing simplicity of adding more functional molecules.[46] All these characteristics provide a unique scaffold that can be effectively used as per our targeted NO detection application.

Published on 02 februari 2023. Downloaded on 20/09/2024 12:59:19.

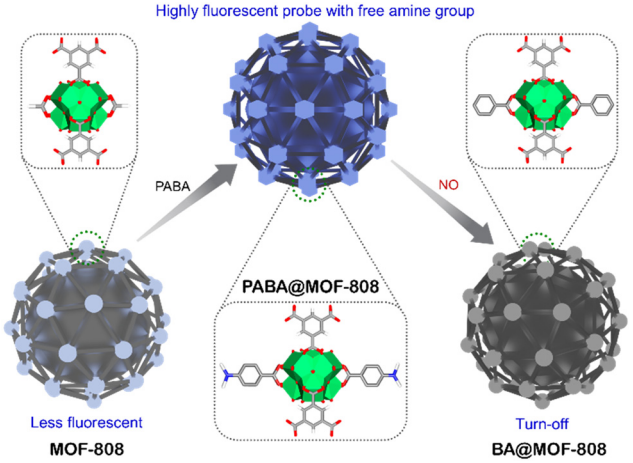

Scheme 1 Schematic illustration of post engineering of a chemically stable MOF and further detection of nitric oxide (NO) with a free amine group containing florescent probe (PABA@MOF-808).

Following these guidelines, herein, we have embraced a chemodosimeter-based approach for demonstrating efficient detection of NO from both aqueous and vapour phases by fabricating a highly stable post-synthetically modified MOF-808-based luminescent probe. It should be mentioned that, unlike chemosensors, the target analyte reacts with the dosimeter (probes) in the chemodosimeter in an irreversible manner to produce signals that are permanent.[47] Because of this, it has been found that both the selectivity and sensitivity toward the target analyte are higher for chemodosimeters in comparison with chemosensors.[48] Therefore, in this work, we have developed a probe by post-synthetic modification of the Zr_6-metal cluster of MOF-808 by coordination grafting with *p*-aminobenzoic acid (PABA) (Scheme 1, Fig. 1a). This strategic engineering of MOF-808 with PABA helps to provide high luminescent nature along with target specific functionality (free amine group) in the probe (PABA@MOF-808). Based on the knowledge that NO reacts with free amine groups,[7] we have deliberately incorporated a free accessible amine group in the framework which can detect NO. Motivated by the strong luminescent nature with high chemical stability, we investigated the detection ability of PABA@MOF-808 towards NO in both water and vapour (Scheme 1). PABA@MOF-808 was found to exhibit highly sensitive and selective detection of NO over other relevant species with superior fluorescence quenching efficiency and low limit of detection (LOD) values. Furthermore, the in-depth mechanism of the fluorescence quenching phenomenon of PABA@MOF-808 by NO was demonstrated with the help of fluorescence resonance energy transfer (FRET), photoinduced electron transfer (PET), density functional theory (DFT) studies and the counter collision process between the fluorescent probe and the analyte. Finally, considering the real-world application, a self-standing, flexible and processable mixed-matrix membrane

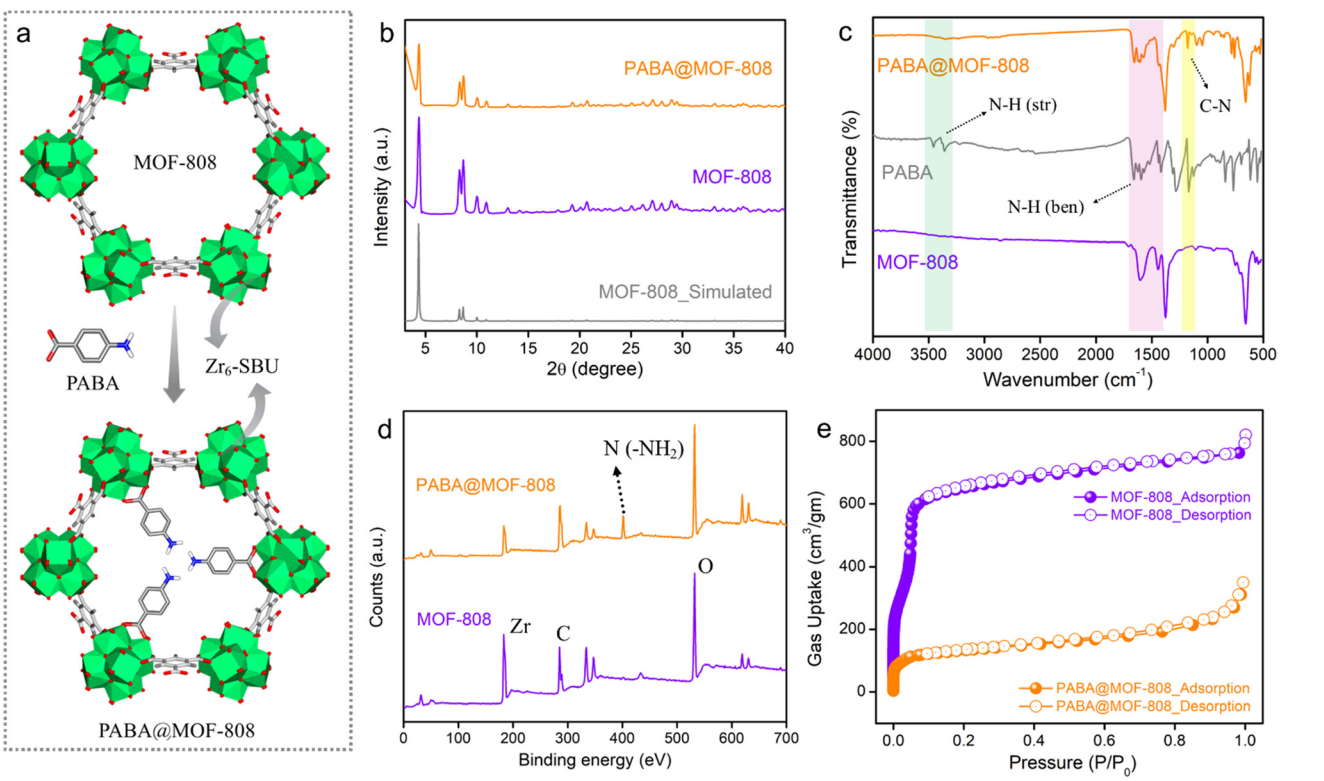

Fig. 1 (a) Schematic representation of post-synthetic modification (PSM) of MOF-808 with *p*-aminobenzoic acid (PABA) (colour code: grey – carbon, white – hydrogen, red – oxygen, blue – nitrogen and green – zirconium). (b) PXRD patterns, (c) FT-IR spectra, (d) XPS survey spectra and (e) nitrogen gas sorption data at 77 K of pristine MOF-808 and PABA@MOF-808.

This journal is © The Royal Society of Chemistry and IChemE 2023

Published on 02 februari 2023. Downloaded on 20/09/2024 12:59:19.

(MMM) of PABA@MOF-808 was fabricated and was further applied for the effective detection of NO from a water medium and qualitative identification from a vapour phase.

Results and discussion

To start, MOF-808 was synthesized *via* a solvothermal reaction according to a reported protocol by reacting its precursors benzene-1,3,5-tricarboxylic acid and $ZrOCl_2 \cdot 8H_2O$.[40] After the synthesis, the powder compound was centrifuged and was washed thrice with DMF followed by water and acetone before being dried in an oven. Preliminary, to check the successful formation, structural integrity and crystallinity of the synthesized compound, the powder X-ray diffraction (PXRD) of the as-synthesized phase was recorded and the pattern was found to well match with the simulated pattern of MOF-808, which indicated the formation of MOF-808 with bulk phase purity (Fig. 1b). Next, to obtain the desolvated phase, the as-synthesized MOF-808 was dipped in methanol for 3–4 days, followed by activation at 100 °C for 12 hours under vacuum. The desolvated MOF-808 was again characterized by PXRD, which suggested similar crystallinity, and the structural integrity was retained in the activated phase (Fig. S1†). The thermogravimetric analysis (TGA) profile of desolvated MOF-808 shows no weight loss up to 240 °C, which indicates that there are no trapped solvent molecules present in the pores of the framework (Fig. S2†). Moreover, the TGA profile exhibits weight losses in two steps of ~11% and ~15%, which are observed in the temperature range of ~267 °C to ~355 °C and ~462 °C to ~614 °C and correspond to the loss of the coordinate formate ion and the 1,3,5-benzenetricarboxylate (BTC) linker, respectively, in the SBU of the MOF.[41,42] Further, Fourier-transform infrared spectroscopy (FT-IR) was applied to characterize MOF-808. Strong absorption bands near 1443 cm^{-1} and 1600 cm^{-1} in the FT-IR spectra correspond to the symmetric and asymmetric stretching frequencies of deprotonated carboxylate groups of the BTC linker of the MOF, respectively (Fig. 1c and S3†).[42,43,46] This suggests the coordination bridging of BTC ligands with Zr(IV)–metal cations. Furthermore, the highly porous nature of MOF-808 was investigated by N_2 sorption measurement at 77 K temperature. The N_2 uptake and corresponding BET surface area for MOF-808 at 1 atm pressure were found to be 763 mL g^{-1} and 2250 m^2 g^{-1}, respectively (Fig. 1e). The pore size distribution (PSD) calculated for MOF-808 through nonlinear density functional theory (NLDFT) using N_2 adsorption data was found to be 2.01 nm (Fig. S4†). After this successful structural characterization, the morphological features of MOF-808 were investigated with the help of field emission scanning electron microscopy (FESEM) analysis. The FESEM images show the regular robust octahedron shape with the smooth surface of the framework (Fig. S5†). Also, the energy dispersive spectroscopy (EDS) with elemental mapping image of MOF-808 shows that C, O, and Zr elements are evenly distributed throughout the compound (Fig. S6†).

After the establishment of the highly crystalline porous structure of MOF-808, it was subjected to post-synthetic modification with *p*-aminobenzoic acid (PABA) to obtain the free amine ($-NH_2$) group containing probe – PABA@MOF-808, following a reported protocol (see the ESI† for details).[46] The thus-synthesized compound was thoroughly characterized with the following techniques. The PXRD pattern of PABA@MOF-808 was found to be identical to that of MOF-808, depicting the similar structural integrity and crystallinity to MOF-808 after the PSM method (Fig. 1b). The TGA profile of PABA@MOF-808 indicated almost the same thermal behaviour as MOF-808 (Fig. S7†). Now, in order to understand the successful coordination grafting of PABA in MOF-808 by the PSM process, FT-IR, Raman, and X-ray photoelectron spectroscopy (XPS) analyses have been done. The IR spectrum of PABA@MOF-808 shows the appearance of a new peak at 1181 cm^{-1}, which corresponds to the stretching frequency of the C–N bond of PABA molecules (Fig. 1c).[46] In addition, the Raman spectrum of PABA@MOF-808 clearly shows a peak associated with the N–H bond of PABA at ~1013 cm^{-1}, which is not present in pure MOF-808 (Fig. S8†).[46] Moreover, the XPS survey spectrum of PABA@MOF-808 presents a peak corresponding to the binding energy of nitrogen atoms at ~401.1 eV compared with that of pristine MOF-808 (Fig. 1d and S9†). All these results validate the successful incorporation of the free $-NH_2$ group in the framework of MOF-808, which is beneficial for the selective NO sensing application. Furthermore, the FESEM images of PABA@MOF-808 revealed that the morphology was found to be identical to that of MOF-808 with a bit rougher surface, which depicted the structural robustness of the post-synthetically modified MOF (Fig. S10†). Moreover, the EDS and elemental mapping analysis of PABA@MOF-808 showed homogeneous distribution of all the relevant C, N, O and Zr elements (Fig. S11†). Further, the N_2 sorption data of PABA@MOF-808 showed a gas uptake amount of 310 mL g^{-1} with a BET surface area of 472 m^2 g^{-1}, which was found to be significantly lower than the pristine MOF-808 (Fig. 1e). This clearly depicted the incorporation of the PABA moiety into the framework.

Now, as aforementioned for real-time aqueous phase detection, a potential sensory material should exhibit high hydrolytic stability. Henceforth to test the water-stability of PABA@MOF-808, it was dipped in water for one week. After 7 days, the material was filtered, dried and characterized with PXRD, TGA, FTIR and FESEM experiments. Both the PXRD pattern and FTIR spectrum of water treated PABA@MOF-808 showed no changes in the peak positions with the pristine compound, depicting retention of structural integrity (Fig. S12 and S13†). The thermogram of the water dipped compound displayed no significant changes suggesting similar thermal stability (Fig. S14†). Moreover, the FESEM images along with EDS and elemental mapping data showed no morphological changes (Fig. S15 and S16a†). Moreover, uniform dispersibility was illustrated by illuminating the MOF solution with a 532 nm laser light which rendered the

Published on 02 februari 2023. Downloaded on 20/09/2024 12:59:19.

Tyndall effect. After 30 min of exposure, the exhibition of the Tyndall effect proves its stability toward the uniform dispersibility of the MOF dispersion (Fig. S16b†).[55] All these results clearly indicated the hydrolytic robustness of PABA@MOF-808 which is advantageous for the practical implementation of the probe for the aqueous phase NO sensing study.

Apart from these structural and morphological characterization results, the optical properties of PABA@MOF-808 were further investigated to check its ability towards sensing application. The solid powder compound was found to have a yellowish colour under the excitation of UV light. The solid-state UV-vis spectrum of PABA@MOF-808 was recorded in the wavelength range of 200 nm to 800 nm, which revealed maximum absorption of light at ~240 nm to ~290 nm (Fig. S17†). Thereafter, the photoluminescence (PL) emission spectrum of water-dispersed PABA@MOF-808 was recorded in the wavelength range of ~300 nm to ~500 nm upon excitation at 290 nm, which exhibited broad emission at 310 nm at room temperature (Fig. S18†). Enthused from these luminescence properties and high structural stability along with the functional recognition moiety (such as the pendant $-NH_2$ group), we sought to investigate the sensing studies with PABA@MOF-808 towards NO in both water and vapour media.

Sensing studies

We have investigated in detail the photoluminescence performances of PABA@MOF-808 towards NO sensing. First, for the detection of nitric oxide, in a typical sensing experiment 1 mg of PABA@MOF-808 was dispersed in 2 ml of water and the corresponding emission spectrum was recorded (Fig. S19a†). After that a certain amount of NO solution (with a concentration of 1 mmol) was added to it and the corresponding emission spectrum was recorded. It was observed that the emission spectrum of the probe was quenched rapidly upon addition of the NO solution (Fig. S20†). In a detailed titration experiment, 1 mM aqueous solution of NO was added by incremental amounts of 20 μL to a total of 300 μL into the PABA@MOF-808/water dispersion. It was found that the fluorescence emission intensity of the probe was gradually quenched upon incremental addition of the NO solution (Fig. 2a). From this fluorescence quenching profile, the quenching constant (K_{sv}) was calculated using the Stern–Volmer equation: $(I_o/I) = 1 + K_{sv}[Q]$, where K_{sv} is the quenching constant, [Q] is the molar concentration of the analyte, and I_o and I are the luminescence intensities before and after addition of the analyte, respectively.[49] The K_{sv} value of PABA@MOF-808 with a linear fitting in a low concentration range for NO sensing was found to be 6.10×10^3 M^{-1} (Fig. 2b). This result explored the strong interaction between the $-NH_2$ group of the probe and NO. Interestingly, this value is found to be one of the best in the domain of MOF-based NO sensing studies.[23] Moreover, for a good sensory material, the limit of detection (LOD) is a necessary parameter in order to evaluate its detection ability for trace concentration.[50] The LOD value calculated for PABA@MOF-808 was 0.715 μM (21.45 ppb) (Fig. 2c). These values clearly indicated the highly sensitive detection of NO molecules by the newly developed

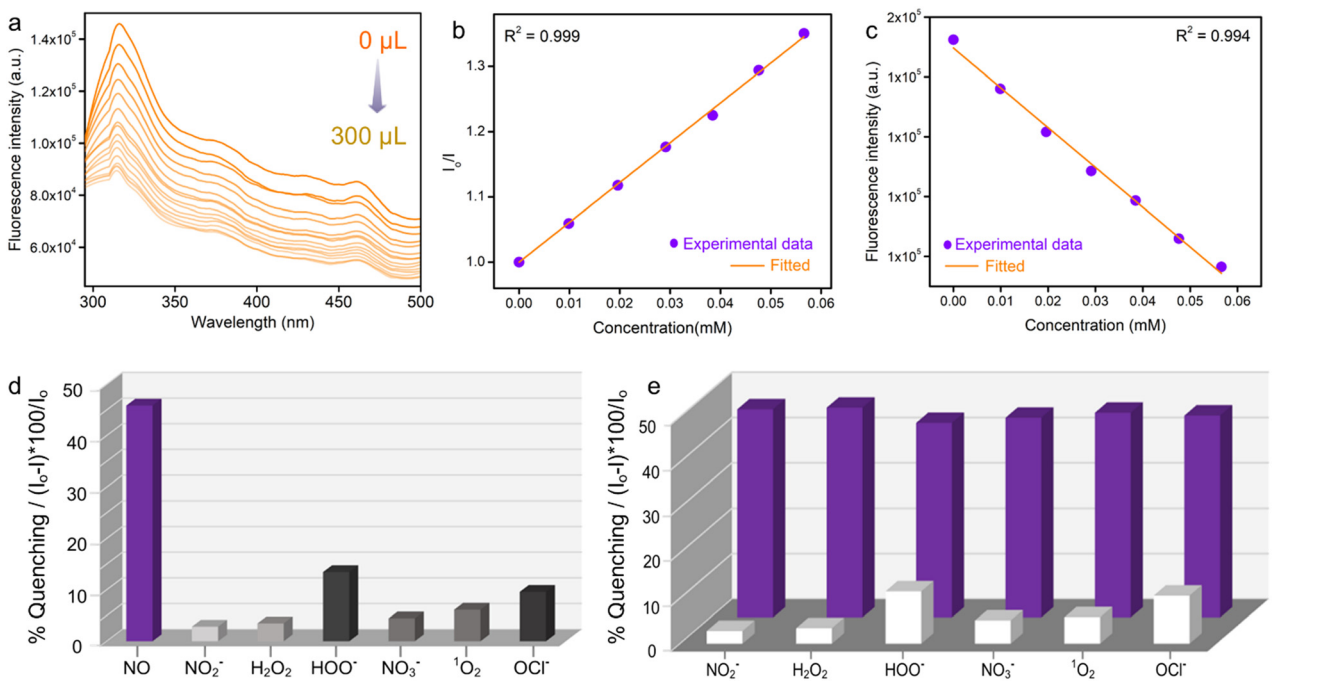

Fig. 2 (a) Photoluminescence spectra of PABA@MOF-808 in water in the presence of different concentrations of NO. (b) Stern–Volmer (SV) plots for quenching of PL intensity of PABA@MOF-808 by NO. (c) LOD calculation plot, (d) relative fluorescence quenching response towards different RNS/ROS in water, and (e) relative fluorescence quenching response towards different RNS/ROS followed by addition of NO solution.

 This journal is © The Royal Society of Chemistry and IChemE 2023

Published on 02 februari 2023. Downloaded on 20/09/2024 12:59:19.

luminescent probe (PABA@MOF-808). On the other hand, apart from sensitivity, selective identification of targeted analytes is an essential criterion for an ideal sensor. Therefore, to test the selectivity of the probe, we have performed the similar sensing study to other relevant interfering reactive nitrogen and oxygen species (RNS or ROS) such as nitrate (NO_3^-), nitrite (NO_2^-), hydrogen peroxide (H_2O_2), singlet oxygen ($^1O_2$), hypochlorite (OCl^-), *etc.* In the single analyte selectivity test, the solution of these species was individually introduced into the aqueous suspension of PABA@MOF-808 and the emission spectra were recorded before and after the addition. It was found that no significant changes in the PL spectra of the PSM-MOF were observed after the addition of these species individually compared to nitric oxide, which confirmed the selective NO detection ability of the probe (Fig. 2d and S21–S26†). This result invigorated us further to perform the binary selectivity detection test of NO in the concurrent presence of the above RNS/ROS species, which is appraised an essential criterion for real world sensing application.

For this experiment, at first we collected the emission spectrum of the pristine PABA@MOF-808/water dispersion followed by the addition of 300 μL interfering analytes (HOO^-, NO_2^-, NO_3^-, H_2O_2, $^1O_2$, OCl^-). Thereafter, again the emission spectrum of the mixture was recorded after introduction of an equal amount of NO solution. As anticipated, the fluorescence intensity of PABA@MOF-808 was found to negligibly quench upon the addition of the aforementioned analytes apart from NO (Fig. S21–S26†). However, interestingly, upon further addition of an equal amount of NO individually into those mixtures, the emission intensity was observed to decrease rapidly (Fig. S21–S26†). This finding confirmed that the coexistence of other relevant species does not disturb the quenching ability of NO for PABA@MOF-808, which further explored its highly selective recognition potential (Fig. 2e). All together, these observations make the current probe applicable for NO detection in complicated real-time biological systems, preventing off-target reactivity and erroneous responses.

Sensing mechanism studies

These results encouraged us further to investigate the in-depth underlying mechanism behind the selective and sensitive detection of NO by PABA@MOF-808. Looking into the literature, it has been found that in general there might be several possibilities of fluorescence quenching, which majorly include rupture of the MOF's structure in the presence of an analyte, diffusional interaction like fluorescence resonance energy transfer (FRET), and non-diffusional interaction like photo induced electron transfer (PET).[9] Now, to explore the mechanism, initially we recorded the PXRD pattern of the NO treated MOF that retained its crystallinity even after completion of the sensing experiment (Fig. S27†). In addition, no changes in the TGA profile as well as FESEM images after the NO treatment of the MOF system indicated the identical thermal stability and robust morphology, respectively (Fig. S28 and S29†). From this observation, we discarded the possibility of quenching of PL emission due to the collapse in the structure of the probe. After this, we focused on the remaining two probable mechanisms *i.e.*, FRET and PET. Resonance energy transfer is an excited state phenomenon that results in dynamic quenching occurring through energy transfer between the fluorophore and the quencher.[23,25,51] To test whether there was any energy transfer between the probe and the analyte (quencher), we compared the absorption spectra of all the analytes and the photoluminescence spectra of the probe. It was found that there was a significant overlap between the PL spectra of the probe and the absorption spectra of nitric oxide (quencher) (Fig. 3a). From this observation, it was quite evident that the energy transfer between PABA@MOF-808 and nitric oxide (NO) is one of the factors in the quenching mechanism. Moreover, we moved ahead to check the photo-induced electron transfer (PET) process as another reason behind this quenching. In the PET process, the excited electron from the probe absorbs light and moves to the analyte's lowest unoccupied molecular orbital (LUMO). Thereafter the probe's ground state is reached by these

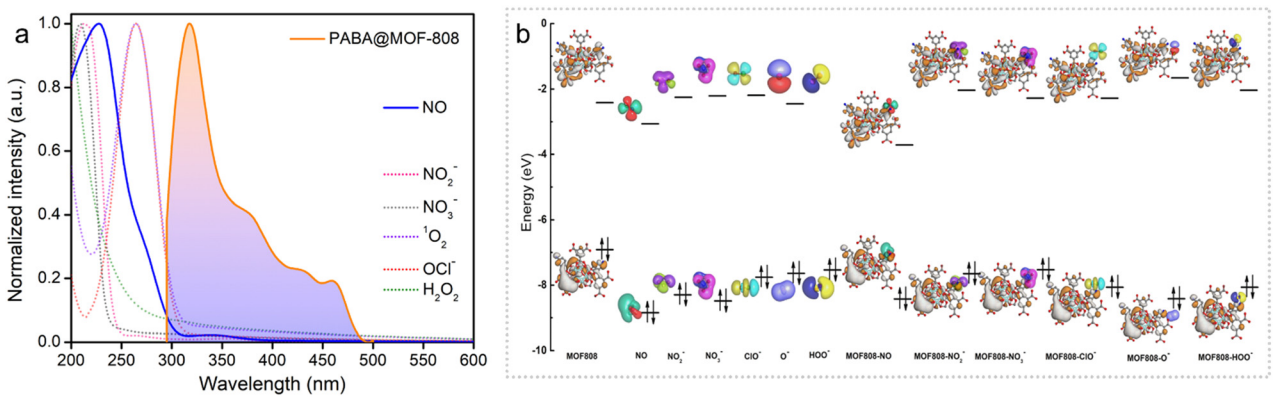

Fig. 3 (a) Spectral overlap between UV-vis spectra of different ROS/RNS and photoluminescence (PL) emission spectra of PABA@MOF-808. (b) HOMO and LUMO energy levels of the PABA@MOF-808 unit and different ROS/RNS along with NO.

Published on 02 februari 2023. Downloaded on 20/09/2024 12:59:19.

excited electrons through a nonradiative drop, which further reduces the fluorescence intensity.[9,51] To test PET, we performed the DFT theoretical calculation, which provided the HOMO–LUMO energy gaps for the PABA@MOF-808 unit and the RNS/ROS including NO using B3LYP-D3/SDD-6-31G(d) (Fig. 3b) (see the ESI† for details). It was found that among all the species, the LUMO of NO lies between the valence band and the conduction band of the probe, which is close to the HOMO of the probe. This enables the electron transfer from the HOMO of PABA@MOF-808 to the LUMO of NO (Fig. 3b). This result validated the photo triggered electron transfer process between NO and PABA@MOF-808 as another plausible mechanism for quenching of fluorescence intensity. Again, to test the nature of the quenching process, lifetime measurement of the probe before and after NO treatment was performed using a time-resolved fluorescence experiment. It was observed that the average lifetime of the probe was slightly changed after the treatment of NO solution (Fig. S30†). This observation suggests the presence of a dynamic quenching process behind the fluorogenic turn-off response.

In addition to this, further we assume that there might be some ground state interaction that operates the quenching mechanism.

To verify this, we performed a solid-state UV-vis spectroscopy study individually with the MOF and NO treated MOF samples. After comparing the absorption spectra of the samples before and after NO addition, it has come to our notice that there is a significant change in the UV-vis spectra with the disappearance of the ~240 nm peak in the case of the NO treated MOF (Fig. S31†). This result clearly suggested that there must be a strong ground-state interaction present between the quencher and the fluorophore. To validate this conclusion, further, we performed ^{1}H NMR and FT-IR studies. The ^{1}H NMR spectra indicated that PABA@MOF-808 exhibited characteristics peaks of the 4-aminobenzoic acids moiety, whereas NO treated PABA@MOF-808 showed the characteristic peaks of benzoic acid (Fig. S32†). Moreover, the FTIR spectra suggested the absence of the peak at ~1181 cm^{-1} in the NO treated sample (Fig. S33†). Also, the XPS spectra indicated the disappearance of the binding energy peak associated with the nitrogen atom in the NO treated MOF powder (Fig. S34†). All these data indicated that NO underwent a fast chemical reaction with the free amino group of the 4-aminobenzoic acid moiety present in the luminescent framework resulting in the formation of benzoic acids and thus the reduction of the luminescent intensity of the probe.[33] All these studies supported the presence of both static and dynamic quenching mechanisms behind the fluorescence-off response of PABA@MOF-808 upon NO addition.

Mixed-matrix-membrane-based sensing studies

Inspired by the above sensing results, we sought to explore the potential of the developed sensor (PABA@MOF-808) towards specific recognition of NO by fabricating a device for the real-time sensing investigation. That being said, although luminescent MOFs in their typical powder form have been extensively studied for the detection of various environmentally relevant chemicals owing to their highly crystalline nature, the full potential of LMOFs towards sensing application is mostly found to be difficult to explore. This is because of the less contact of the probe with the analyte solution due to the nonhomogeneous dispersion of the powder MOFs. Such a phenomenon broadly restricts the maximum probe–analyte interactions which further creates less sensitivity and low detection ability as well as inaccuracy in the sensing result.[9,10,52] Therefore, it is particularly important to develop processable forms of LMOFs for the practical sensing application. In this regard, fabrication of LMOF-based membranes or films, or more especially mixed-matrix-membranes (MMMs), is recently considered as a promising strategy for various potential applications.[53] Although, in recent years, significant research has been conducted to demonstrate MOF-based films or membranes for various utilizations, LMOF-based MMMs towards detection of toxic NO gas have largely been unexplored. The development of MOF-based MMMs offers manipulation, easy handling, flexibility and processability of the materials for the practical application. Furthermore, the superior crack resistance ability, high flexibility and processability allow them to be molded into different device forms.[54] Moreover, the homogeneous distribution of the probes (LMOFs) throughout a large area of the MMM offers high solvent permeation flux and exposed most of the interactive sites of the probe towards upcoming analytes. This increases the analyte–probe (LMOFs) interaction to enhance the sensitivity of the detection.[54]

Keeping all the consideration in mind, in this work, we developed a mixed-matrix-membrane based on a composite mixture of PABA@MOF-808 with a widely used polymer, poly(vinylidene fluoride) [PVDF] and further used it for efficient detection of nitric oxides in a gaseous phase as well as in an aqueous medium. We have adopted the well-known drawdown coating (doctor-blading) method for the fabrication of luminescent MMMs. In a typical procedure, at first a suspension of PVDF in DMF solvent was prepared. Then a certain amount of PABA@MOF-808 was mixed in the above suspension and a homogeneous dispersion was made by mixing overnight. Thereafter, this mixture was cast onto Al-foil by hand with the help of a glass substrate to make homogeneous films. Next, these coated PABA@MOF-808@PVDF films were heated on a hot-plate to finally prepare the self-standing MMMs as schematically represented in Fig. 4a (see the ESI† for details). It is noteworthy to mention that in order to understand the role of the amount of MOFs in the NO sensing study, a series of MMMs have been fabricated with the similar above protocol taking different loading contents of PABA@MOF-808 (20, 40, 60, 80 and 100 wt% (in mg)) in the PVDF solution. The thus-developed MMMs were found to be self-standing, macroscopic defect or

 This journal is © The Royal Society of Chemistry and IChemE 2023

Published on 02 februari 2023. Downloaded on 20/09/2024 12:59:19.

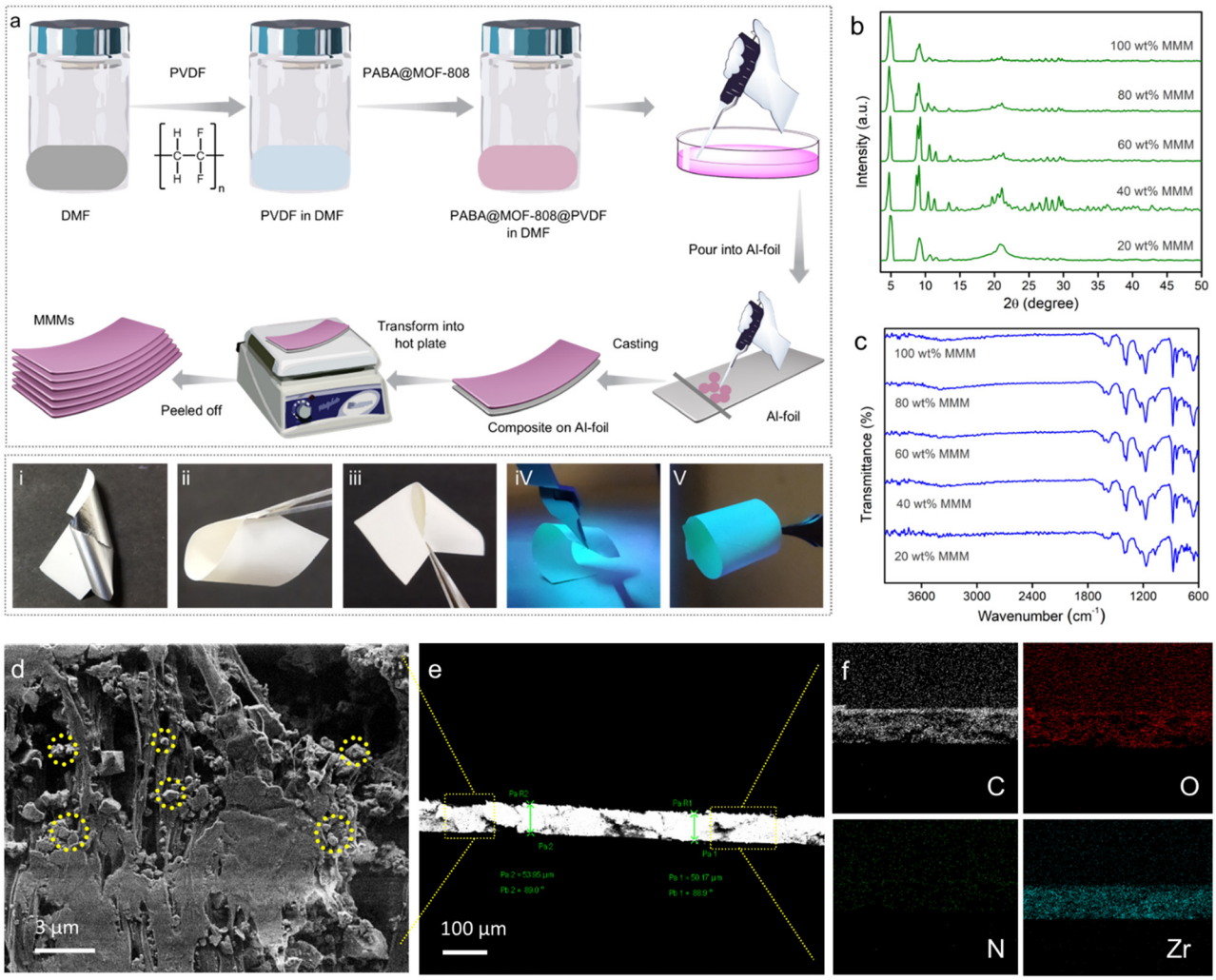

Fig. 4 (a) Schematic illustration of the MMM fabrication procedure by the drawdown coating (doctor-blading) method. (b) PXRD patterns and (c) FT-IR spectra of the PABA@MOF-808@PVDF MMMs with different MOF ratios. (i–v) Digital images of the 80 wt% MMM showing its self-standing, mechanical stability and highly luminescent nature under UV light. (d) FESEM top view image of the 80 wt% MMM. (e) FESEM cross-section image of the 80 wt% MMM. (f) FESEM elemental mapping images of the respective elements (C: carbon, O: oxygen, N: nitrogen, Zr: zirconium).

crack free, mechanically stable and highly luminescent in nature, which are beneficial for the real-time NO sensing study (Fig. 4(i–v)). After the fabrication, the MMMs were thoroughly characterized by PXRD, FT-IR, TGA and FESEM analyses. The PXRD patterns of all the MMMs indicated the presence of highly crystalline PABA@MOF-808 with no structural changes in the PVDF composite (Fig. 4b). Further, upon increasing the amount of the MOF nanocrystals in the MMMs the amorphous nature of the PVDF polymer is weakened and consequently, the peaks of the MOFs become sharp (Fig. 4b). This result suggests the robust structural integrity with bulk purity of the probe in the MMMs. The corresponding distinguished peaks in the FT-IR spectra of all the MMMs clearly indicated the stable existence of PABA@MOF-808 bound with the PVDF polymer (Fig. 4c). The TGA profiles of the MMMs revealed the improved thermal behaviour compared to the pristine powder materials because of the high thermal stability of the PVDF polymer (Fig. S35†). After this structural characterization, the morphological investigation has been done with the help of FESEM analysis. As a representative example, we selected the 80 wt% MMM for this analysis. The front view of the FESEM images of the PABA@MOF-808@PVDF MMM clearly showed the presence of the octahedral morphology of the MOFs throughout the polymeric phase of the PVDF membrane (Fig. 4d and S36†). Moreover, intact robustness of the sensing probe along with the minimal aggregation of MOF particles can be observed from the FESEM images (Fig. 4f and S37†). In addition, the cross-section images of the MMM showed a thickness of ~60 to ~80 µm (Fig. 4e and S38†). The energy dispersive X-ray spectroscopy (EDS) analysis indicated the presence of all the relevant elements along with zirconium (Zr) and nitrogen (N), which suggests successful grafting of PABA@MOF-808 in the PVDF membrane (Fig. S39†). Also, these elements were found to homogeneously distribute throughout the large surface of the membrane, which suggests no obvious aggregation of

Published on 02 februari 2023. Downloaded on 20/09/2024 12:59:19.

MOF nanoparticles (Fig. 4f and S40†). Furthermore, the porous nature of this MMM was confirmed from the nitrogen gas sorption measurement at 77 K, which provided the surface area to be 62.76 m^2 g^{-1} (Fig. S41†). These data also indicated lowering of the total gas uptake and thus reduction in the surface area compared to the powder MOF samples.[52]

After the successful characterization, we moved ahead to perform the NO sensing studies by these MMMs both from aqueous and vapour phases. From a preliminary screening test, it was observed that the MMM made up with 80 wt% PABA@MOF-808 exhibited the highest emission intensity under excitation of 290 nm UV radiation (Fig. S42†). Now, the above sensing study and the insight mechanism reveal that upon treatment of NO, the amino benzoic acid group of the highly luminescent probe (PABA@MOF-808) converted into a benzoic acid group, which is found to be less luminescent in nature. Therefore, in order to test the feasibility of the developed MMM towards efficient detection of NO, we have performed a titration study for aqueous phase sensing. At first, the emission profile of the 80% MMM was recorded, which exhibited a broad spectrum with a maximum at ~325 nm upon excitation at ~290 nm (Fig. S42†). Interestingly, the high emission intensity of the MMM was found to be significantly quenched when treated with 1 mmol aqueous NO solution. Motivated by this observation, we adopted a typical soaking method for the thorough titration sensing study.

In this method, a small piece of the MMM was dipped into different concentrations of aqueous solution of the salt for a certain time, and the respective fluorescence intensities were recorded before and after NO treatment. It was found that upon dipping of the MMM into the NO solution, the high emission intensity of the MMM decreased gradually with increasing concentration. From Fig. 5a, it was calculated that nearly about 59% emission intensity of the MMM was quenched upon treatment of 220 μL of 1 mmol NO solution. This quenching phenomenon of the MMMs can also be visualized from the digital images (Fig. 5-viii). Thereafter, from this fluorescence quenching profile the quenching constant (K_{sv}) was calculated. The K_{sv} value of the MMM for NO was found to be 4.15×10^3 M^{-1} (Fig. S43†). Furthermore, the LOD value of this MMM was calculated to be 0.715 μM (Fig. S44†). Both these K_{sv} and LOD values of the MMM for NO sensing were also found to be well comparable with the other literature reports. Along with high sensitivity, the selective detection of targeted species is also an important parameter for an effective sensor. Therefore, we performed the selectivity test of the MMM for NO sensing along with the other aforementioned interferences with the similar soaking method. As anticipated, the MMM was found to exhibit a qualitative quenching response in the case of NO only, whereas, other interferences were observed to be unable to change the emission intensity of the MMM (Fig. 5(i–viii)). These results clearly indicated the potential of the

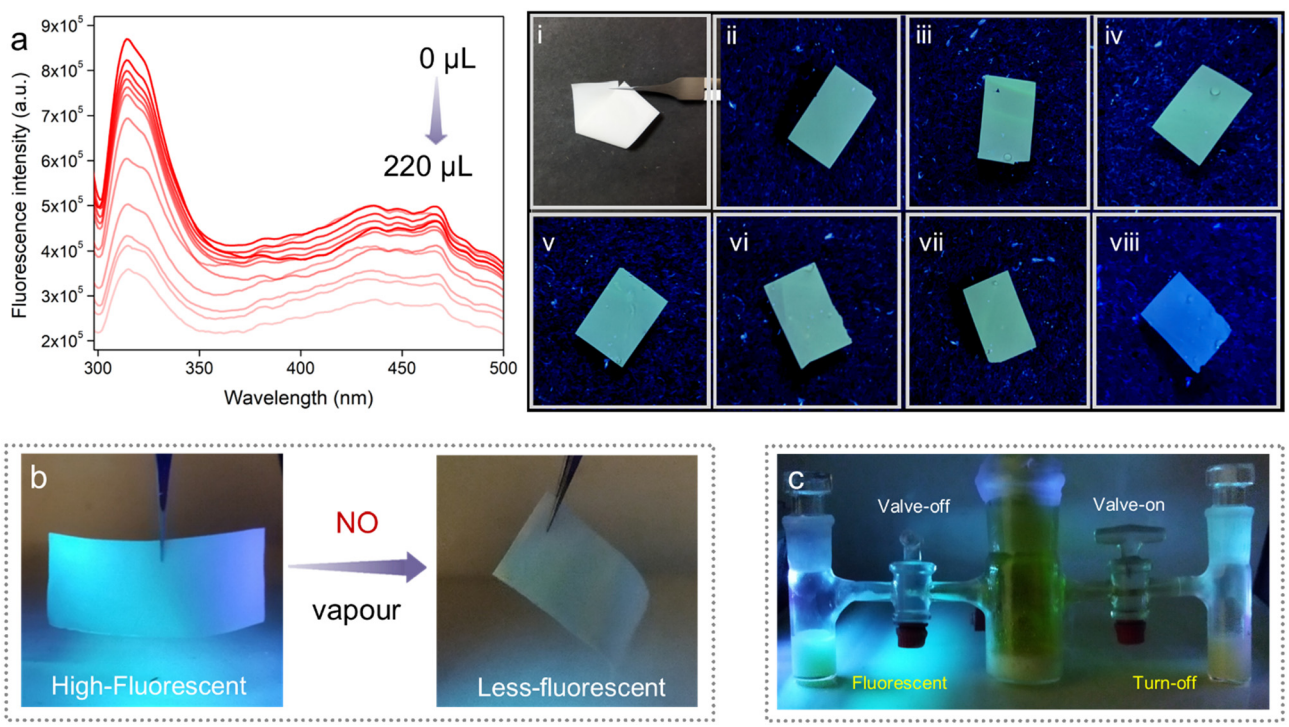

Fig. 5 (a) Photoluminescence spectra of the PABA@MOF-808-MMM in water in the presence of different concentrations of NO. (i) Pristine MMM, (ii) H_2O_2, (iii) $^1O_2$, (iv) NO_2^-, (v) NO_3^-, (vi) OCl^-, (vii) HOO^-, and (viii) NO treated MMM. (b) Digital images of the luminescence quenching response of the self-standing MMMs upon treatment with NO vapour, under UV light. (c) Demonstration of the "turn-off" behaviour of PABA@MOF-808/water in contact with NO vapour.

 This journal is © The Royal Society of Chemistry and IChemE 2023

Published on 02 februari 2023. Downloaded on 20/09/2024 12:59:19.

PABA@MOF-808-based MMM towards real-time aqueous phase selective and sensitive NO sensing. Enthused by the above results, as a proof of concept, we also looked at the practical application and proceeded to investigate the vapour phase NO sensing by the MMM. As a quantitative test, we made a set-up for the demonstration of vapour phase NO detection by the self-standing MMM (Fig. S45†). As shown in Fig. 5b, the MMM in the prototype device exhibited rapid identification of NO gas generated from the reaction of KI and $NaNO_2$ (see the ESI† for details). A similar turn-off response was observed in the case of aqueous suspension of the powder sample upon exposure to NO vapour (Fig. 5c). This impressive finding suggested a potential use for the PABA@MOF-808-based MMMs in both aqueous and vapour phase practical detection of toxic NO. The improved sensitivity of the MMM towards NO might be the cause of triggered interactions between the NO molecules and functional recognition sites of the sensor, which are generated due to the homogenous distribution of the probe throughout the membrane matrix.

Conclusions

To summarize, in this work we have presented a straightforward way of crafting functionality tailored MOFs to act as a molecular flask for monitoring the presence of NO. The judiciously chosen amine group bearing organic linker was introduced inside the porous cavity of the MOF-808 Zr-SBU cluster *via* post-synthetic modification as a versatile tool to yield PABA@MOF-808. The thus-prepared amine functionalized MOF was found to show rapid and sensitive recognition of NO in the dual phase. Aside from fluorescence quenching through a "turn-off" signal response, the presence of NO could also be seen under UV light by the naked eye. The potency of PABA@MOF-808 is further highlighted by its high K_{sv} value (6.10×10^3 M^{-1}) and excellent LOD of 0.715 μM. Further, the sensing response was exclusive toward the target analyte even in the presence of interfering RNS/ROS making it a superior sensory probe. To gain mechanistic understanding of NO detection, in-depth experimental and DFT theoretical studies were also carried out. Keeping in mind the practical applicability, a self-standing flexible mixed-matrix membrane was also fabricated for qualitative NO sensing in water as well as in the vapour phase. We believe that this work can actuate further research in developing task-specific functionalized MOF based sensory materials with the objective of accomplishing suitable probes for detecting biologically important molecules.

Author contributions

W. M. and S. K. G. designed the project. W. M. wrote the manuscript. W. M., D. M. and S. F. collected and analysed the data. S. L. and S. F. helped in the manuscript preparation. S. F. prepared the graphical materials. M. M. S. did the theoretical studies. S. K. G. supervised the project and revised the manuscript. All authors have given permission to the final version of the manuscript.

Conflicts of interest

There are no conflicts to declare.

Acknowledgements

W. M. and D. M. thank the IISER Pune for research fellowships. S. F. acknowledges the DST-Inspire (India) for the research fellowship (DST/INSPIRE/03/2016/001694). S. L. is thankful to the CSIR India for the research fellowship. M. M. S. thanks the SIU Pune, India for the technical support. We are grateful to the IISER Pune for its research facilities. S. K. G. thanks the DST-SERB project (Project No. CRG/2019/000906) for funding.

References

1 P. N. Coneski and M. H. Schoenfisch, *Chem. Soc. Rev.*, 2012, **41**, 3753–3758.
2 P. G. Wang, M. Xian, X. Tang, X. Wu, Z. Wen, T. Cai and A. J. Janczuk, *Chem. Rev.*, 2002, **102**, 1091.
3 M. H. Lim and S. J. Lippard, *Acc. Chem. Res.*, 2007, **40**, 41–51.
4 X. Hu, J. Wang, X. Zhu, D. Dong, X. Zhang, S. Wu and C. Duan, *Chem. Commun.*, 2011, **47**, 11507–11509.
5 J. Garthwaite, S. L. Charles and R. Chess-Williams, *Nature*, 1988, **336**, 385.
6 V. Calabrese, C. Mancuso, M. Calvani, E. Rizzarelli, D. A. Butterfield and A. M. G. Stella, *Nat. Rev. Neurosci.*, 2007, **8**, 766.
7 T. Nagano and T. Yoshimura, *Chem. Rev.*, 2002, **102**, 1235.
8 E. A. Dolgopolova, A. M. Rice, C. R. Martin and N. B. Shustova, *Chem. Soc. Rev.*, 2018, **47**, 4710–4728.
9 S. Fajal, W. Mandal, D. Majumder, M. M. Shirolkar, Y. D. More and S. K. Ghosh, *Chem. – Eur. J.*, 2022, **28**, e202104175.
10 W. Mandal, S. Fajal, P. Samanta, S. Dutta, M. M. Shirolkar, Y. D. More and S. K. Ghosh, *ACS Appl. Polym. Mater.*, 2022, **4**(11), 8633–8644.
11 E. Sasaki, H. Kojima, H. Nishimatsu, Y. Urano, K. Kikuchi, Y. Hirata and T. Nagano, *J. Am. Chem. Soc.*, 2005, **127**, 3684–3685.
12 H. Yu, Y. Xiao and L. Jin, *J. Am. Chem. Soc.*, 2012, **134**, 17486–17489.
13 Y. Yang, S. K. Seidlits, M. M. Adams, V. M. Lynch, C. E. Schmidt, E. V. Anslyn and J. B. Shear, *J. Am. Chem. Soc.*, 2010, **132**, 13114–13116.
14 Y.-Q. Sun, J. Liu, H. Zhang, Y. Huo, X. Lv, Y. Shi and W. Guo, *J. Am. Chem. Soc.*, 2014, **136**, 12520–12523.
15 M. H. Lim, D. Xu and S. J. Lippard, *Nat. Chem. Biol.*, 2006, **2**, 375–380.
16 Y. Chen, W. Guo, Z. Ye, G. Wang and J. Yuan, *Chem. Commun.*, 2011, **47**, 6266.
17 A. Schoedel, M. Li, D. Li, M. O'Keeffe and O. M. Yaghi, *Chem. Rev.*, 2016, **116**, 12466–12535.

Published on 02 februari 2023. Downloaded on 20/09/2024 12:59:19.

18 Z. Chen, S. L. Hanna, L. R. Redfern, D. Alezi, T. Islamoglu and O. K. Farha, *Coord. Chem. Rev.*, 2019, **386**, 32–49.
19 S. Rojas and P. Horcajada, *Chem. Rev.*, 2020, **120**(16), 8378–8415.
20 Y. Bai, Y. B. Dou, L. H. Xie, W. Rutledge, J. R. Li and H. C. Zhou, *Chem. Soc. Rev.*, 2016, **45**, 2327–2367.
21 T. N. Tu, M. V. Nguyen, H. L. Nguyen, B. Yuliarto, K. E. Cordova and S. Demir, *Coord. Chem. Rev.*, 2018, **364**, 33–50.
22 S. K. Ghosh, *Metal-Organic Frameworks (MOFs) for Environmental Applications*, Elsevier, 2019, DOI: **10.1016/C2017-0-01721-4**.
23 W. P. Lustig, S. Mukherjee, N. D. Rudd, A. V. Desai, J. Li and S. K. Ghosh, *Chem. Soc. Rev.*, 2017, **46**, 3242–3285.
24 Z. C. Hu, B. J. Deibert and J. Li, *Chem. Soc. Rev.*, 2014, **43**, 5815–5840.
25 P. Samanta, S. Let, W. Mandal, S. Dutta and S. K. Ghosh, *Inorg. Chem. Front.*, 2020, **7**, 1801–1821.
26 Y. Zhang, S. Yuan, G. Day, X. Wang, X. Yang and H.-C. Zhou, *Coord. Chem. Rev.*, 2018, **354**, 28–45.
27 S. Nagarkar, A. V. Desai and S. K. Ghosh, *Chem. – Eur. J.*, 2015, **21**, 9994–9997.
28 A. Karmakar, B. Joarder, A. Mallick, P. Samanta, A. V. Desai, S. Basu and S. K. Ghosh, *Chem. Commun.*, 2017, **53**, 1253.
29 D. Mahato, S. Fajal, P. Samanta, W. Mandal and S. K. Ghosh, *ChemPlusChem*, 2022, **87**, e2021004.
30 S. Mukherjee, S. Dutta, Y. D. More, S. Fajal and S. K. Ghosh, *Dalton Trans.*, 2021, **50**, 17832–17850.
31 S. Dutta, Y. D. More, S. Fajal, W. Mandal, G. K. Dam and S. K. Ghosh, *Chem. Commun.*, 2022, **58**, 13676–13698.
32 Y. Chen, W. Guo, Z. Ye, G. Wanga and J. Yuan, *Chem. Commun.*, 2011, **47**, 6266–6268.
33 A. V. Desai, P. Samanta, B. Manna and S. K. Ghosh, *Chem. Commun.*, 2015, **51**, 6111–6114.
34 A. Beltrán, M. I. Burguete, D. R. Abánades, D. Pérez-Sala, S. V. Luis and F. Galindo, *Chem. Commun.*, 2014, **50**, 3579–3581.
35 P. Wu, J. Wang, C. He, X. Zhang, Y. Wang, T. Liu and C. Duan, *Adv. Funct. Mater.*, 2012, **22**, 1698–1703.
36 J. Wang, Y. Yin, Q. Rao, G. Li, W. Sun, F. X. Hu and C. M. Li, *ACS Appl. Nano Mater.*, 2022, **5**(2), 2451–2459.
37 B. J. Privett, J. H. Shinb and M. H. Schoenfisch, *Chem. Soc. Rev.*, 2010, **39**, 1925–1935.
38 S. Jiang, R. Cheng, X. Wang, T. Xue, Y. Liu, A. Nel, Y. Huang and X. Duan, *Nat. Commun.*, 2013, **4**, 2225.
39 M. D. Brown and M. H. Schoenfisch, *Chem. Rev.*, 2019, **119**, 11551–11575.
40 J. Jiang, F. Gandara, Y.-B. Zhang, K. Na and O. M. Yaghi, *J. Am. Chem. Soc.*, 2014, **136**, 12844–12847.
41 L. H. T. Nguyen, T. T. Nguyen, H. L. Nguyen, T. L. H. Doan and P. H. Tran, *Catal. Sci. Technol.*, 2017, **7**, 4346–4350.
42 A. Singh, S. Karmakar, I. M. Abraham, D. Rambabu, D. Dave, R. Manjithaya and T. K. Maji, *Inorg. Chem.*, 2020, **59**, 8251–8258.
43 S. Karmakar, A. Ghosh, F. A. Rahimi, B. Rawat and T. K. Maji, *ACS Appl. Mater. Interfaces*, 2022, **14**, 49014–49025.
44 H.-Y. Zhang, Y. Yang, C.-C. Li, H.-L. Tang, F.-M. Zhang, G.-L. Zhang and H. Yan, *J. Mater. Chem. A*, 2021, **9**, 16743–16750.
45 S. Li, Y. Zhou and B. Yan, *Inorg. Chem.*, 2022, **61**(25), 9615–9622.
46 R. Thur, D. V. Havere, N. V. Velthoven, S. Smolders, A. Lamaire, J. Wieme, V. V. Speybroeck, D. D. Vos and I. F. J. Vankelecom, *J. Mater. Chem. A*, 2021, **9**, 12782–12796.
47 M. E. Jun, B. Roy and K. H. Ahn, *Chem. Commun.*, 2011, **47**, 7583–7601.
48 P. Samanta, A. V. Desai, S. Sharma, P. Chandra and S. K. Ghosh, *Inorg. Chem.*, 2018, **57**, 2360–2364.
49 S. Fajal, P. Samanta and S. K. Ghosh, *Inorg. Chim. Acta*, 2020, **502**, 119359.
50 S. Let, P. Samanta, S. Dutta and S. K. Ghosh, *Inorg. Chim. Acta*, 2020, **500**, 119205.
51 B. Wang, Q. Yang, C. Guo, Y. Sun, L.-H. Xie and J.-R. Li, *ACS Appl. Mater. Interfaces*, 2017, **9**, 10286–10295.
52 X. Zhang, Q. Zhang, D. Yue, J. Zhang, J. Wang, B. Li, Y. Yang, Y. Cui and G. Qian, *Small*, 2018, **14**, 1801563.
53 Y. Cheng, S. J. Datta, S. Zhou, J. Jia, O. Shekhah and M. Eddaoudi, *Chem. Soc. Rev.*, 2022, **51**, 8300–8350.
54 M. S. Denny and S. M. Cohen, *Angew. Chem., Int. Ed.*, 2015, **54**, 9029–9032.
55 A. Nath, G. M. Thomas, S. Hans, S. R. Vennapusa and S. Mandal, *Inorg. Chem.*, 2022, **61**, 2227–2233.
56 S. Mandal, S. Natarajan, P. Mani and A. Pankajakshan, *Adv. Funct. Mater.*, 2020, **31**, 2006291.
57 A. Nath, K. S. Asha and S. Mandal, *Chem. – Eur. J.*, 2021, **27**, 11482–11538.

 This journal is © The Royal Society of Chemistry and IChemE 2023